Supporting Information

Platinum(II) Dihalide Complexes with 9-Arsafluorenes: Effects of Ligand Modification on the Phosphorescent Properties

Hiroaki Imoto[†], Hiroshi Sasaki[†], Susumu Tanaka[†], Takashi Yumura[‡], and Kensuke Naka[*,†]

[†] Faculty of Molecular Chemistry and Engineering, Graduate School of Science and Technology, Kyoto Institute of Technology, Goshokaido-cho, Matsugasaki, Sakyo-ku, Kyoto 606-8585, Japan.
[‡] Faculty of Materials Science and Engineering, Graduate School of Science and Technology, Kyoto Institute of Technology, Goshokaido-cho, Matsugasaki, Sakyo-ku, Kyoto 606-8585, Japan.

Contents:

1. Crystallographic data

Table S1. Crystallographic Data of *cis*- and *trans*-[$PtCl_2$(**2**)$_2$].

	cis-[$PtCl_2$(**2**)$_2$]	*trans*-[$PtCl_2$(**2**)$_2$]
Crystal data		
Empirical Formula	C26H22As2Cl2Pt	C26H22As2Cl2Pt
Formula Weight	750.30	750.30
Crystal Dimension, mm^3	0.400 × 0.300 × 0.200	0.430 × 0.100 × 0.030
Crystal System	monoclinic	Orthorhombic
Space Group	C2/c	$P2_1/c$
a, Å	17.622(8)	6.636(6)
b, Å	10.998(4)	17.828(14)
c, Å	14.564(6)	10.361(16)
α, deg	-	-
β, deg	122.715(4)	106.668(10)
γ, deg	-	-
Volume, $Å^3$	2374.8(17)	1174.3(16)
D_{calcd}, g cm^{-3}	2.098	2.122
Z	4	2
F(000)	1424	712
Data Collection		
Temperature, deg	25.0	25.0
2θmax, deg	55.0	54.9
Tmin/Tmax	0.0773 / 0.198	0.470 / 0.827
Refinement		
No. of Observed Data	2559	2699
No. of Parameters	141	142
R1[a], wR2[b]	0.0277, 0.0548	0.0360, 0.0756
Goodness of Fit Indictor	0.818	1.097

[a] $R1 = \Sigma \, | \, |Fo| - |Fc| \, | \, / \, \Sigma \, |Fo|$ [b] $wR2 = [\, \Sigma \, w \, ((Fo^2-Fc^2)^2 \, / \, \Sigma \, w \, (Fo^2)^2 \,]^{1/2}$ $w = [\, \sigma^2(Fo^2) \,]^{-1}$

CCDC # 1539989 (*cis*-[$PtCl_2$(**2**)$_2$]) and 1539988 (*trans*-[$PtCl_2$(**2**)$_2$])

Table S2. Crystallographic Data of *trans*-[$PtBr_2$(**2**)$_2$] and *trans*-[PtI_2(**2**)$_2$].

	trans-[$PtBr_2$(**2**)$_2$]	*trans*-[PtI_2(**2**)$_2$]
Crystal data		
Empirical Formula	C26H22As2Br2Pt	C26H22As2I2Pt
Formula Weight	839.20	933.20
Crystal Dimension, mm^3	0.370 × 0.060 × 0.060	0.170 × 0.090 × 0.080
Crystal System	monoclinic	monoclinic
Space Group	$P2_1/c$	$P2_1/c$
a, Å	6.6795(9)	6.739(5)
b, Å	18.0804(19)	18.694(12)
c, Å	10.4380(13)	10.532(7)
α, deg	-	-
β, deg	106.999(6)	107.906(9)
γ, deg	-	-
Volume, $Å^3$	1205.5(3)	1262.5(15)
D_{calcd}, g cm^{-3}	2.312	2.455
Z	2	2
F(000)	784	856.00
Data Collection		
Temperature, deg	25.0	25.0
2θmax, deg	55.0	54.9
Tmin/Tmax	0.229 / 0.865	0.296 / 0.506
Refinement		
No. of Observed Data	2764	2859
No. of Parameters	142	142
R1[a], wR2[b]	0.0408, 0.1072	0.0401, 0.0944
Goodness of Fit Indictor	0.930	1.073

[a] $R1 = \Sigma \, | \, |Fo| - |Fc| \, | \, / \, \Sigma \, |Fo|$ [b] $wR2 = [\, \Sigma \, w \, ((Fo^2-Fc^2)^2 \, / \, \Sigma \, w \, (Fo^2)^2 \,]^{1/2}$ $w = [\, \sigma^2(Fo^2) \,]^{-1}$

CCDC # 1539990 (*trans*-[$PtBr_2$(**2**)$_2$]) and 1540001 (*trans*-[PtI_2(**2**)$_2$])

Table S3. Crystallographic Data of $[PtX_2(\mathbf{3})_2]$ (X = Cl, Br, and I)

	cis-$[PtCl_2(\mathbf{3})_2]$	*cis*-$[PtBr_2(\mathbf{3})_2]$	*trans*-$[PtI_2(\mathbf{3})_2]$
Crystal data			
Empirical Formula	C32H34As2Cl2Pt	C33H36As2Br2Cl2Pt	C22H34As2I2Pt
Formula Weight	834.46	1008.29 [c]	1017.36
Crystal Dimension, mm^3	0.210 × 0.140 × 0.080	0.372 × 0.236 × 0.207	0.204 × 0.008 × 0.003
Crystal System	monoclinic	monoclinic	monoclinic
Space Group	$P2_1/c$	$P2_1/n$	$P2_1/n$
a, Å	9.49 (5)	10.4292(7)	13.132(6)
b, Å	15.84 (9)	16.0838(8)	7.348(4)
c, Å	20.41(11)	21.3211(12)	17.053(8)
α, deg	-	-	-
β, deg	103.06(6)	95.513(3)	102.239(6)
γ, deg	-	-	-
Volume, $Å^3$	2990(29)	3559.9(3)	1608.2(14)
D_{calcd}, g cm^{-3}	1.854	1.881	2.101
Z	4	4	2
F(000)	1616	1928	952
Data Collection			
Temperature, deg	25.0	25.0	25.0
2θmax, deg	55.1	55.0	55.0
Tmin/Tmax	0.296 / 0.505	0.068 / 0.241	0.327 / 0.694
Refinement			
No. of Observed Data	6737	8155	3692
No. of Parameters	334	370	169
R1[a], wR2[b]	0.0399, 0.0969	0.0693, 0.2397	0.0348, 0.0799
Goodness of Fit Indictor	1.005	1.069	1.037

[a] $R1 = \Sigma \, | \, |Fo| - |Fc| \, | \, / \, \Sigma \, |Fo|$ [b] $wR2 = [\, \Sigma \, w \, ((Fo^2-Fc^2)^2 \, / \, \Sigma \, w \, (Fo^2)^2 \,]^{1/2}$ $w = [\, \sigma^2(Fo^2) \,]^{-1}$

[c] included solvent, CH_2Cl_2

CCDC # 1539991 (*cis*-$[PtCl_2(\mathbf{3})_2]$), 1539993 (*cis*-$[PtBr_2(\mathbf{3})_2]$), and 1539992 (*trans*-$[PtI_2(\mathbf{3})_2]$)

Table S4. Crystallographic Data of $[PtCl_2(\mathbf{4})_2]$

	cis-$[PtCl_2(\mathbf{4})_2]$	*trans*-$[PtCl_2(\mathbf{4})_2]$
Crystal data		
Empirical Formula	C36H38As2Cl2Pt	C36H38As2Cl2Pt
Formula Weight	886.54	886.54
Crystal Dimension, mm^3	0.300 × 0.110 × 0.060	0.290 × 0.110 × 0.050
Crystal System	orthorhombic	monoclinic
Space Group	Pbca	C2/c
a, Å	18.7472(16)	17.942(2)
b, Å	16.4843(15)	9.0338(9)
c, Å	22.3213(19)	22.568(2)
α, deg	-	-
β, deg	-	94.935(6)
γ, deg	-	-
Volume, $Å^3$	6898.1(11)	3644.5(7)
D_{calcd}, g cm^{-3}	1.707	1.616
Z	8	4
F(000)	3456	1728
Data Collection		
Temperature, deg	25.0	25.0
2θmax, deg	55.2	55.1
Tmin/Tmax	0.239 / 0.680	0.313 / 0.761
Refinement		
No. of Observed Data	7965	4186
No. of Parameters	370	187
R1[a], wR2[b]	0.0427, 0.0533	0.43, 0.1063
Goodness of Fit Indictor	1.171	0.996

[a] $R1 = \Sigma \, | \, |Fo| - |Fc| \, | \, / \, \Sigma \, |Fo|$ [b] $wR2 = [\, \Sigma \, w \, ((Fo^2-Fc^2)^2 \, / \, \Sigma \, w \, (Fo^2)^2 \,]^{1/2}$ $w = [\, \sigma^2(Fo^2) \,]^{-1}$

CCDC # 1539999 (*cis*-$[PtCl_2(\mathbf{4})_2]$) and 1539995 (*trans*-$[PtCl_2(\mathbf{4})_2]$)

Table S5. Crystallographic Data of $[PtX_2(\mathbf{4})_2]$ (X = Br and I)

	cis-$[PtBr_2(\mathbf{4})_2]$	*trans*-$[PtBr_2(\mathbf{4})_2]$	*trans*-$[PtI_2(\mathbf{4})_2]$
Crystal data			
Empirical Formula	C36H38As2Br2Pt	C36H38As2Br2Pt	C36H38As2I2Pt
Formula Weight	975.44	975.44	1069.44
Crystal Dimension, mm^3	0.250 × 0.070 × 0.020	0.450 × 0.080 × 0.080	0.024 × 0.210 × 0.010
Crystal System	orthorhombic	triclinic	monoclinic
Space Group	Pbca	P-1	$P2_1/n$
a, Å	18.853(6)	9.0138(9)	12.9350(14)
b, Å	16.567(6)	13.9403(19)	16.5587(19)
c, Å	22.434(8)	13.9995(19)	16.2154(18)
α, deg	-	89.543(18)	-
β, deg	-	84.889(12)	99.048(6)
γ, deg	-	84.468(16)	-
Volume, $Å^3$	7007(4)	1744.0(4)	3429.9(7)
D_{calcd}, g cm^{-3}	1.849	1.857	2.071
Z	8	2	4
F(000)	3744.00	936.00	2016
Data Collection			
Temperature, deg	25.0	25.0	25.0
2θmax, deg	55.0	55.3	55.0
Tmin/Tmax	0.269 0.867	0.144 / 0.527	0.217 / 0.626
Refinement			
No. of Observed Data	71501	8014	7866
No. of Parameters	8047	373	370
R1[a], wR2[b]	0.0905, 0.2877	0.0697, 0.2141	0.0451, 0.1043
Goodness of Fit Indictor	1.048	1.065	0.944

[a] $R1 = \Sigma \mid |Fo| - |Fc| \mid / \Sigma |Fo|$ [b] $wR2 = [\ \Sigma\, w ((Fo^2-Fc^2)^2 / \Sigma\, w (Fo^2)^2\ ]^{1/2}$ $w = [\ \sigma^2(Fo^2)\ ]^{-1}$

CCDC # 1540000 (*cis*-$[PtBr_2(\mathbf{4})_2]$), 1539994 (*trans*-$[PtBr_2(\mathbf{4})_2]$), and 1539997 (*trans*-$[PtI_2(\mathbf{4})_2]$)

Table S6. Crystallographic Data of $[PtX_2(\mathbf{5})_2]$ (X = Cl and I)

	cis-$[PtCl_2(\mathbf{5})_2]$	*trans*-$[PtI_2(\mathbf{5})_2]$
Crystal data		
Empirical Formula	C38H30As2Cl2O2Pt	C36H38As2I2O2Pt
Formula Weight	934.49	1119.41
Crystal Dimension, mm^3	0.170 × 0.120 × 0.010	0.230 × 0.110 × 0.080
Crystal System	triclinic	triclinic
Space Group	Pbca	P-1
a, Å	8.9902(10)	9.13510(16)
b, Å	9.1496(10)	10.3622(6)
c, Å	21.117(2)	11.7498(4)
α, deg	94.216(3)	83.781(10)
β, deg	92.699(4)	74.428(10)
γ, deg	106.267(6)	78.586(10)
Volume, $Å^3$	1658.8(3)	1048.42(9)
D_{calcd}, g cm^{-3}	1.871	1.773
Z	2	1
F(000)	904.00	526
Data Collection		
Temperature, deg	25.0	25.0
2θmax, deg	55.0	55.0
Tmin/Tmax	0.372 / 0.857	0.340 / 0.573
Refinement		
No. of Observed Data	7579	4791
No. of Parameters	406	205
R1[a], wR2[b]	0.0436, 0.0599	0.0282, 0.0333
Goodness of Fit Indictor	0.930	0.822

[a] $R1 = \Sigma \, | \, |Fo| - |Fc| \, | \, / \, \Sigma \, |Fo|$ [b] $wR2 = [\, \Sigma \, w \, ((Fo^2-Fc^2)^2 \, / \, \Sigma \, w \, (Fo^2)^2 \,]^{1/2}$ $w = [\, \sigma^2(Fo^2) \,]^{-1}$

CCDC # 1539998 (*cis*-$[PtCl_2(\mathbf{5})_2]$) and 1539996 (*trans*-$[PtI_2(\mathbf{5})_2]$)

Table S7. ORTEP drawing (ellipsoids at 50% probability), selected distances (Å), and angles (deg) of *cis*-[$PtCl_2$(**2**)$_2$].

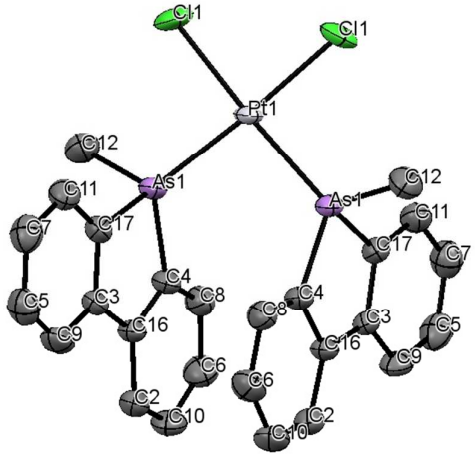

distances (Å)		angles (°)	
Pt(1)-As(1)	2.3434(7)	As(1)-Pt(1)-As(1)	95.97(2)
Pt(1)-Cl(2)	2.320(1)	As(1)-Pt(1)-Cl(1)	87.57(4)
As(1)-C(12)	1.942(5)	Cl(1)-Pt(1)-Cl(1)	88.89(5)
		Pt(1)-As(1)-C(12)	115.6(2)

Table S8. ORTEP drawing (ellipsoids at 50% probability), selected distances (Å), and angles (deg) of *trans*-[$PtCl_2$(**2**)$_2$].

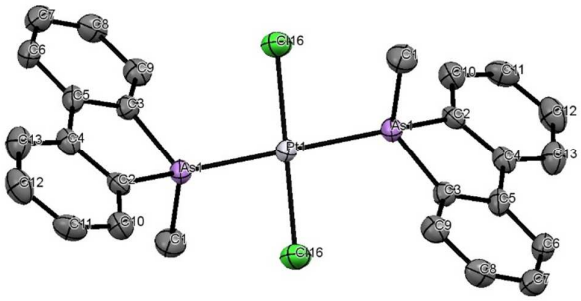

distances (Å)		angles (°)	
Pt(1)-As(1)	2.394(1)	As(1)-Pt(1)-Cl(16)	87.56(5)
Pt(1)-Cl(16)	2.302(2)	As(1)-Pt(1)-Cl(16)	92.44(5)
As(1)-C(1)	1.930(7)	C(1)-As(1)-Pt(1)	116.1(2)

Table S9. ORTEP drawing (ellipsoids at 50% probability), selected distances (Å), and angles (deg) of *trans*-[$PtBr_2$(**2**)$_2$].

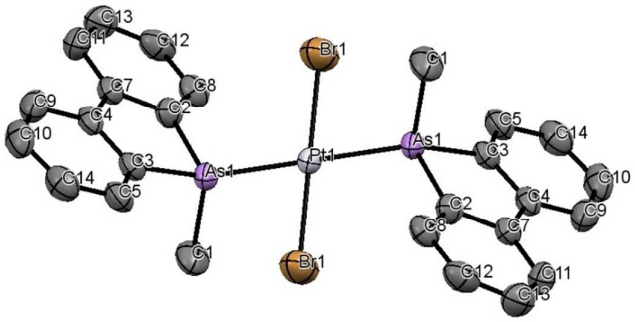

distances (Å)		angles (°)	
Pt(1)-As(1)	2.3907(7)	As(1)-Pt(1)-Br(1)	87.78(3)
Pt(1)-Br(1)	2.413(1)	As(1)-Pt(1)-Br(1)	92.22(3)
As(1)-C(1)	1.947(9)	C(1)-As(1)-Pt(1)	116.4(3)

Table S10. ORTEP drawing (ellipsoids at 50% probability), selected distances (Å), and angles (deg) of *trans*-[PtI_2(**2**)$_2$].

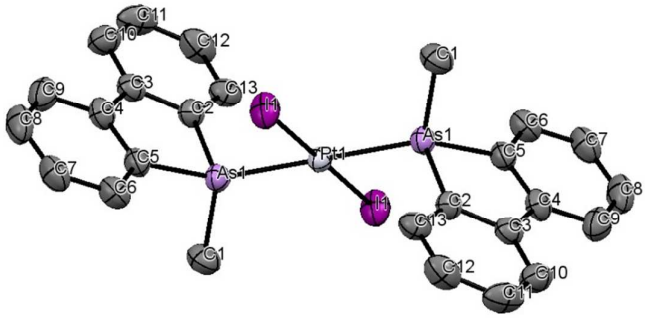

distances (Å)		angles (°)	
Pt(1)-As(1)	2.395(1)	I(1)-Pt(1)-As(1)	88.13(2)
Pt(1)-I(1)	2.593(1)	I(1)-Pt(1)-As(1)	91.87(2)
As(1)-C(1)	1.928(7)	C(1)-As(1)-Pt(1)	118.3(2)

Table S11. ORTEP drawing (ellipsoids at 50% probability), selected distances (Å), and angles (deg) of *cis*-[$PtCl_2$(**3**)$_2$].

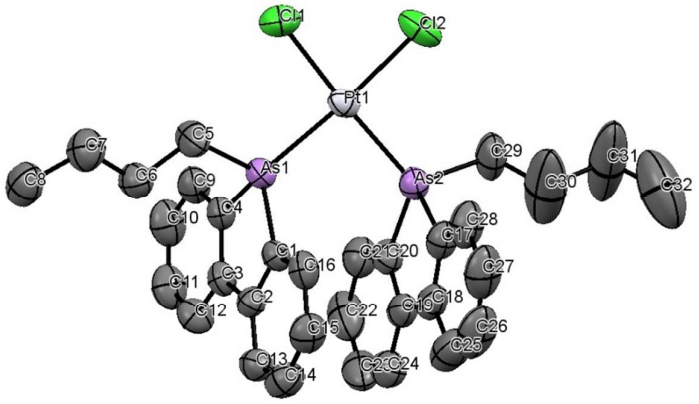

distances (Å)		angles (°)	
Pt(1)-As(1)	2.35(1)	As(1)-Pt(1)-As(2)	94.11(2)
Pt(1)-As(2)	2.35(1)	As(1)-Pt(1)-Cl(1)	88.74(5)
Pt(1)-Cl(1)	2.32(1)	As(2)-Pt(1)-Cl(2)	89.68(5)
Pt(1)-Cl(2)	2.33(1)	Cl(1)-Pt(1)-Cl(2)	87.60(7)
As(1)-C(5)	1.95(1)	C(5)-As(1)-Pt(1)	115.9(2)
As(2)-C(29)	1.95(1)	C(29)-As(2)-Pt(1)	116.0(2)

Table S12. ORTEP drawing (ellipsoids at 50% probability), selected distances (Å), and angles (deg) of *cis*-[$PtBr_2$(**3**)$_2$].

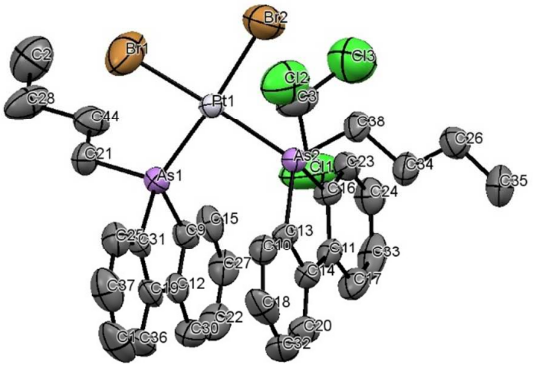

distances (Å)		angles (°)	
Pt(1)-As(1)	2.342(1)	As(1)-Pt(1)-As(2)	92.75(4)
Pt(1)-As(2)	2.3447(9)	As(1)-Pt(1)-Br(1)	88.08(7)
Pt(1)-Br(1)	2.406(2)	As(2)-Pt(1)-Br(2)	91.29(5)
Pt(1)-Br(2)	2.398(2)	Br(1)-Pt(1)-Br(2)	88.90(8)
As(1)-C(21)	1.93(1)	C(21)-As(1)-Pt(1)	115.2(4)
As(2)-C(38)	1.94(1)	C(38)-As(2)-Pt(1)	114.9(4)

Table S13. ORTEP drawing (ellipsoids at 50% probability), selected distances (Å), and angles (deg) of *trans*-[PtI_2(**3**)$_2$].

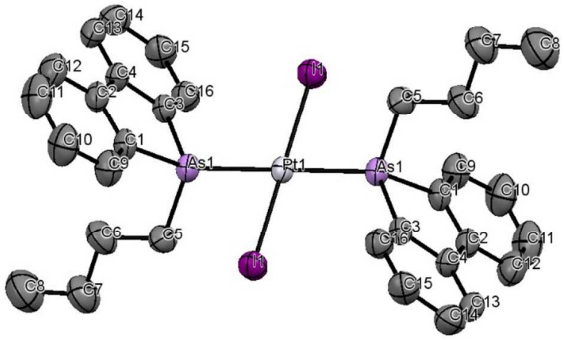

distances (Å)		angles (°)	
Pt(1)-As(1)	2.396(1)	I(1)-Pt(1)-As(1)	87.89(2)
Pt(1)-I(1)	2.605(1)	I(1)-Pt(1)-As(1)	92.11(2)
As(1)-C(5)	1.946(7)	C(5)-As(1)-Pt(1)	115.9(2)

Table S14. ORTEP drawing (ellipsoids at 50% probability), selected distances (Å), and angles (deg) of *cis*-[$PtCl_2$(**4**)$_2$].

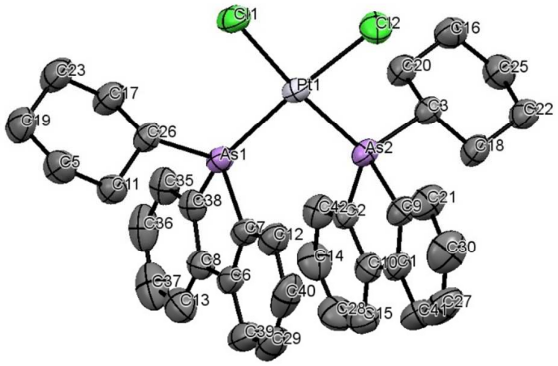

distances (Å)		angles (°)	
Pt(1)-As(1)	2.3433(7)	As(1)-Pt(1)-As(2)	93.83(2)
Pt(1)-As(2)	2.3403(6)	As(1)-Pt(1)-Cl(1)	91.54(4)
Pt(1)-Cl(1)	2.326(1)	As(2)-Pt(1)-Cl(2)	87.17(4)
Pt(1)-Cl(2)	2.341(2)	Cl(1)-Pt(1)-Cl(2)	88.05(5)
As(1)-C(26)	1.964(5)	C(26)-As(1)-Pt(1)	115.3(1)
As(2)-C(3)	1.952(5)	C(3)-As(2)-Pt(1)	112.7(1)

Table S15. ORTEP drawing (ellipsoids at 50% probability), selected distances (Å), and angles (deg) of *trans*-[$PtCl_2$(**4**)$_2$].

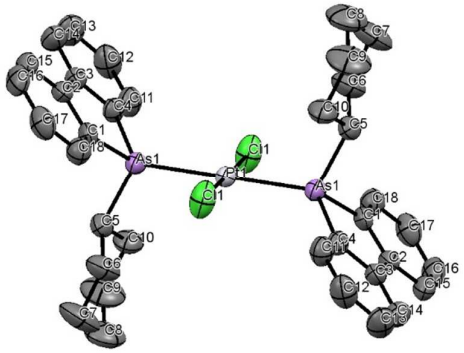

distances (Å)		angles (°)	
Pt(1)-As(1)	2.4031(5)	Cl(1)-Pt(1)-As(1)	89.94(5)
Pt(1)-Cl(1)	2.290(2)	Cl(1)-Pt(1)-As(1)	90.06(5)
As(1)-C(5)	1.969(5)	C(5)-As(1)-Pt(1)	112.4(2)

Table S16. ORTEP drawing (ellipsoids at 50% probability), selected distances (Å), and angles (deg) of *cis*-[$PtBr_2$(**4**)$_2$].

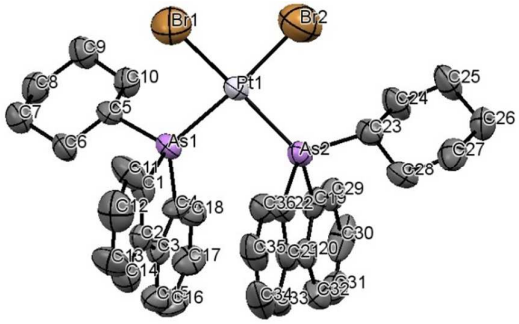

distances (Å)		angles (°)	
Pt(1)-As(1)	2.349(2)	As(1)-Pt(1)-As(2)	93.79(5)
Pt(1)-As(2)	2.351(2)	As(1)-Pt(1)-Br(1)	87.50(9)
Pt(1)-Br(1)	2.401(4)	As(2)-Pt(1)-Br(2)	91.0(1)
Pt(1)-Br(2)	2.382(4)	Br(1)-Pt(1)-Br(2)	88.5(1)
As(1)-C(5)	1.94(2)	C(5)-As(1)-Pt(1)	113.7(4)
As(2)-C(23)	1.97(2)	C(23)-As(2)-Pt(1)	115.4(4)

Table S17. ORTEP drawing (ellipsoids at 50% probability), selected distances (Å), and angles (deg) of *trans*-[$PtBr_2$(**4**)$_2$].

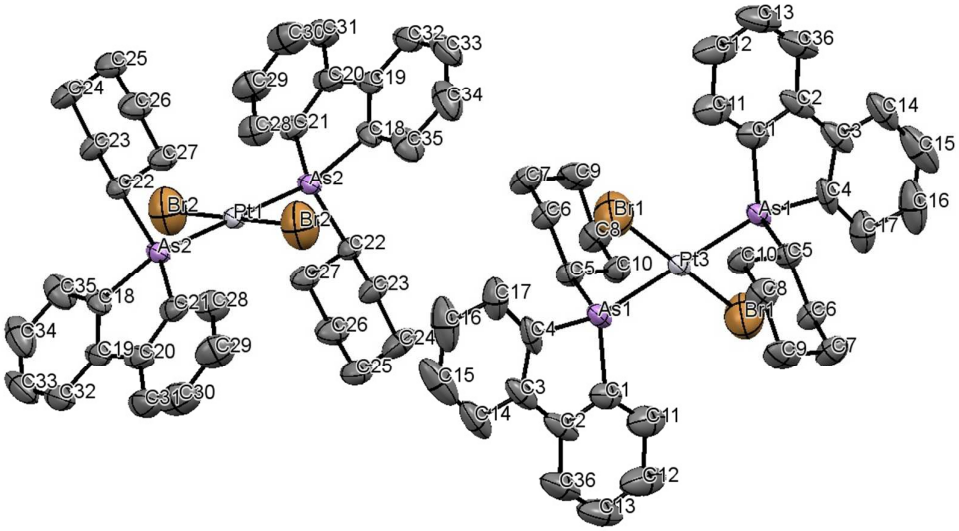

distances (Å)		angles (°)	
Pt(1)-As(2)	2.402(1)	As(2)-Pt(1)-Br(2)	89.13(7)
Pt(3)-As(1)	2.393(1)	As(2)-Pt(1)-Br(2)	90.87(7)
Pt(1)-Br(2)	2.355(3)	As(1)-Pt(3)-Br(1)	90.37(7)
Pt(2)-Br(1)	2.361(2)	As(1)-Pt(3)-Br(1)	89.63(7)
As(2)-C(22)	1.97(1)	C(22)-As(2)-Pt(1)	111.8(3)
As(1)-C(5)	1.96(1)	C(5)-As(1)-Pt(3)	111.2(3)

Table S18. ORTEP drawing (ellipsoids at 50% probability), selected distances (Å), and angles (deg) of *trans*-[PtI_2(**4**)$_2$].

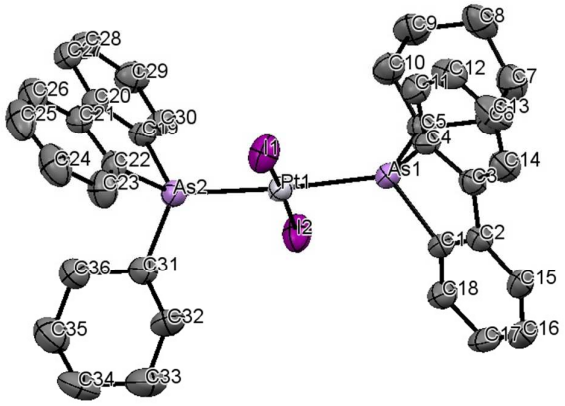

distances (Å)		angles (°)	
Pt(1)-As(1)	2.4038(7)	As(1)-Pt(1)-I(1)	92.63(2)
Pt(1)-As(2)	2.4026(7)	As(1)-Pt(1)-I(2)	87.98(2)
Pt(1)-I(1)	2.5894(7)	As(2)-Pt(1)-I(1)	91.89(2)
Pt(1)-I(2)	2.6130(7)	As(2)-Pt(1)-I(2)	88.00(2)
As(1)-C(5)	1.974(7)	C(5)-As(1)-Pt(1)	112.5(2)
As(2)-C(31)	1.948(7)	C(31)-As(2)-Pt(1)	116.1(2)

Table S19. ORTEP drawing (ellipsoids at 50% probability), selected distances (Å), and angles (deg) of *cis*-[$PtCl_2$(**5**)$_2$].

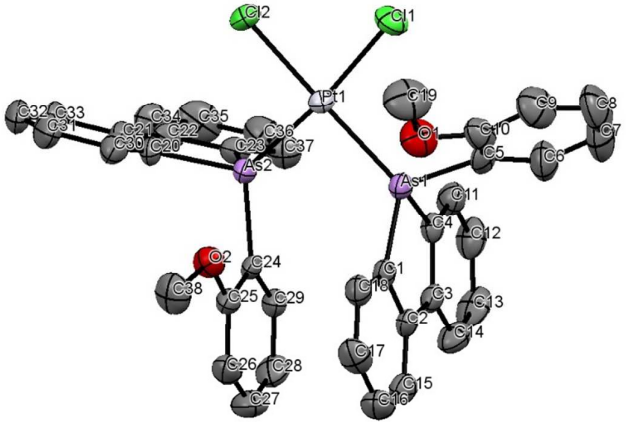

distances (Å)		angles (°)	
Pt(1)-As(1)	2.3501(7)	As(1)-Pt(1)-As(2)	96.22(2)
Pt(1)-As(2)	2.3464(8)	As(1)-Pt(1)-Cl(1)	90.93(5)
Pt(1)-Cl(1)	2.334(2)	As(2)-Pt(1)-Cl(2)	83.57(4)
Pt(1)-Cl(2)	2.324(1)	Cl(1)-Pt(1)-Cl(2)	89.09(6)
As(1)-C(5)	1.951(7)	C(5)-As(1)-Pt(1)	116.5(2)
As(2)-C(24)	1.944(5)	C(24)-As(2)-Pt(1)	122.6(2)

Table S20. ORTEP drawing (ellipsoids at 50% probability), selected distances (Å), and angles (deg) of *trans*-[PtI_2(**5**)$_2$].

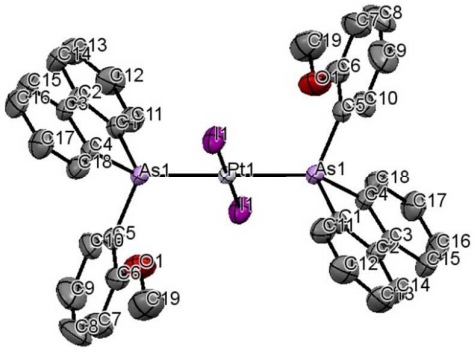

distances (Å)		angles (°)	
Pt(1)-As(1)	2.3916(5)	I(1)-Pt(1)-As(1)	87.10(1)
Pt(1)-I(1)	2.5969(4)	I(1)-Pt(1)-As(1)	92.90(1)
As(1)-C(5)	1.934(5)	C(5)-As(1)-Pt(1)	115.3(1)

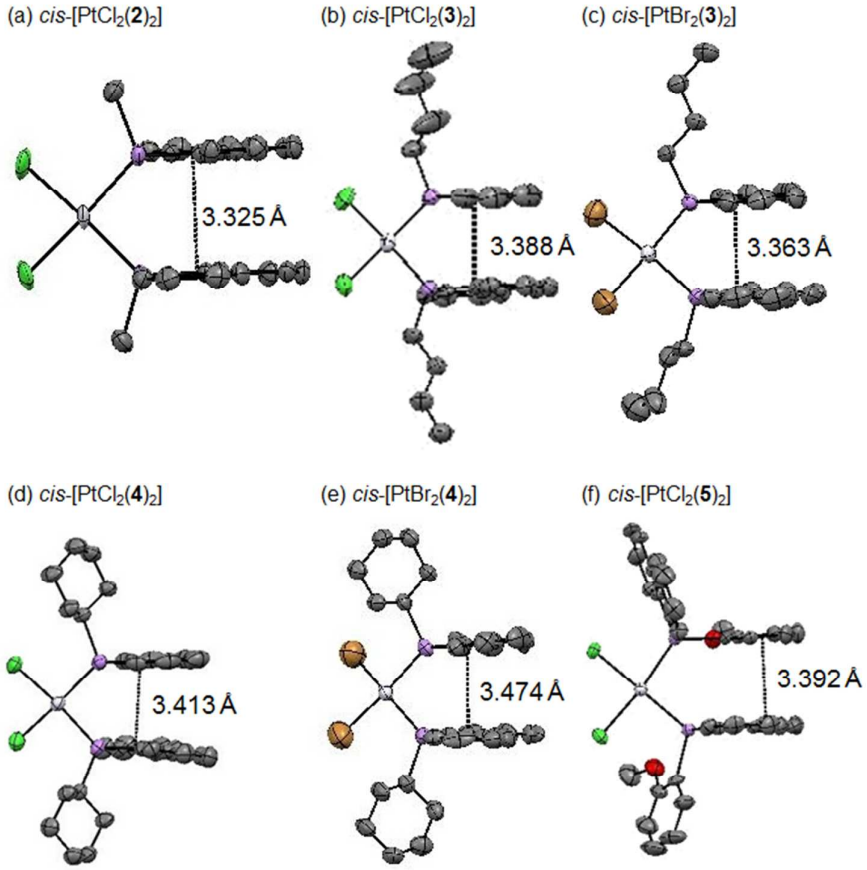

Figure S1. Intramolecular π-π interactions in *cis*-complexes.

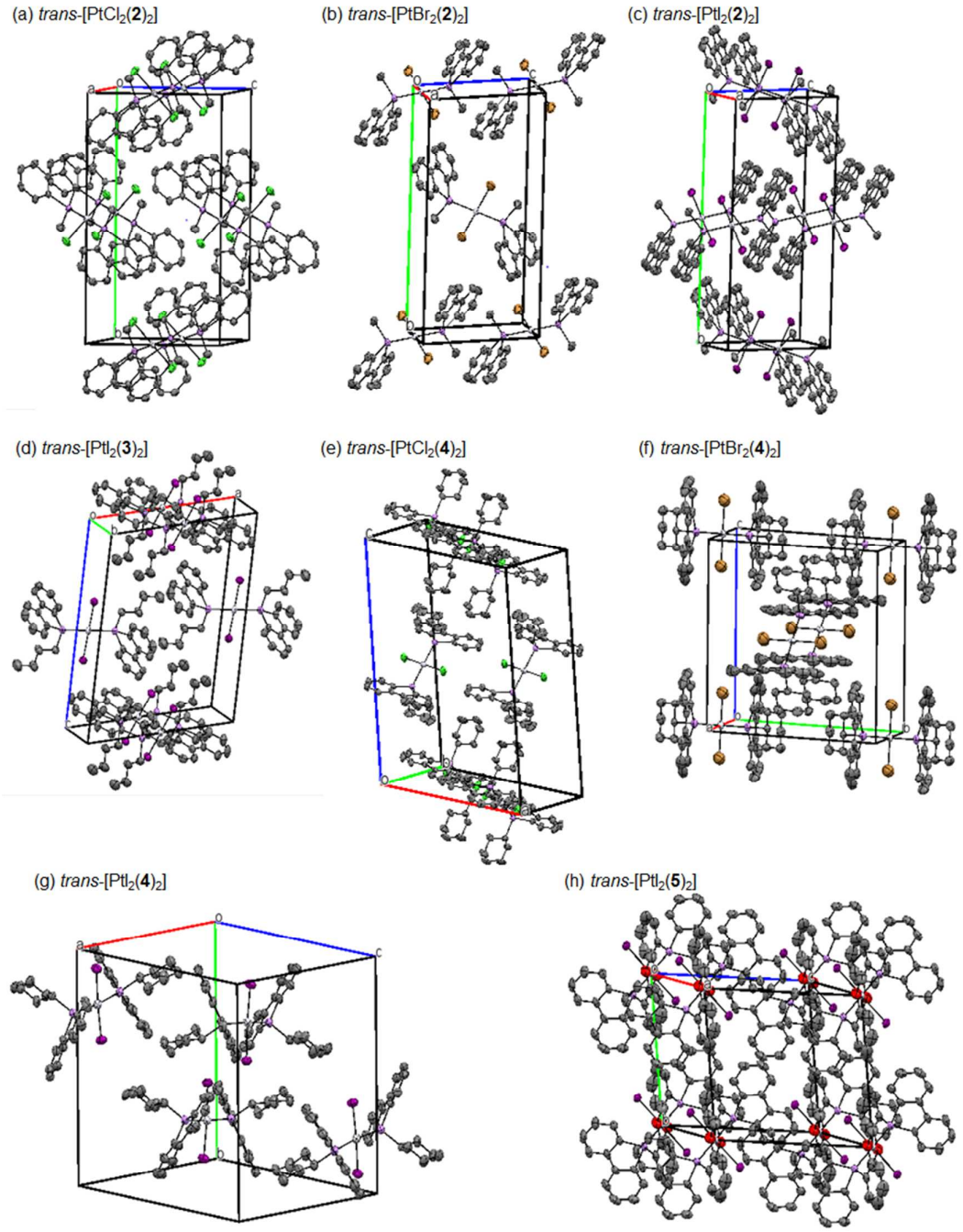

Figure S2. Packing structures of *trans*-complexes.

2. NMR spectra

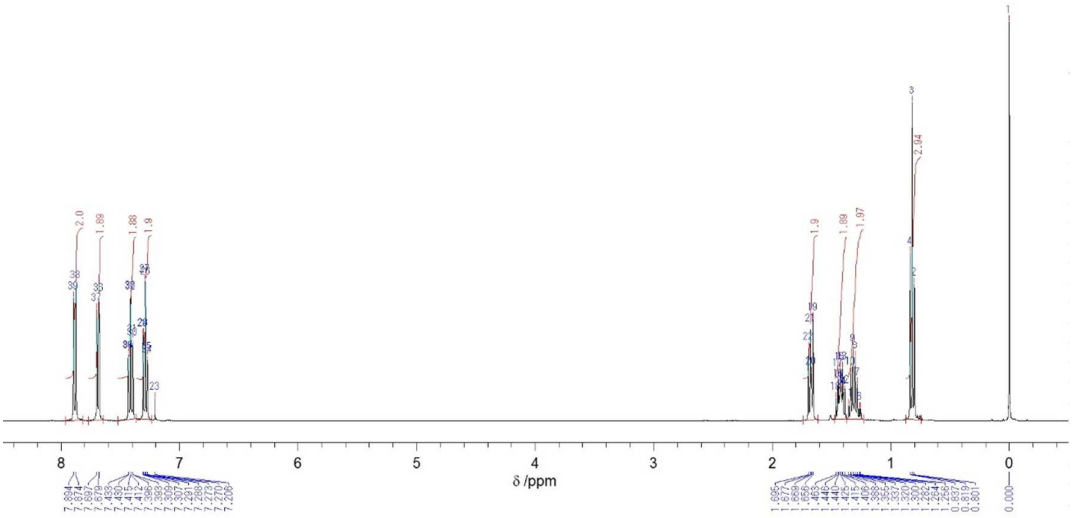

Figure S3. ^{1}H NMR spectrum (400 MHz) of **3** in $CDCl_3$.

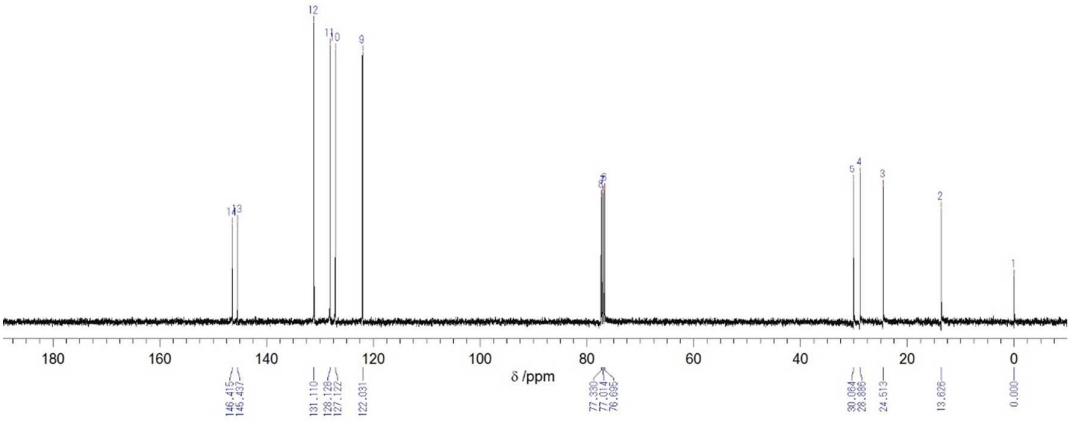

Figure S4. $^{13}C\{^{1}H\}$ NMR spectrum (100 MHz) of **3** in $CDCl_3$.

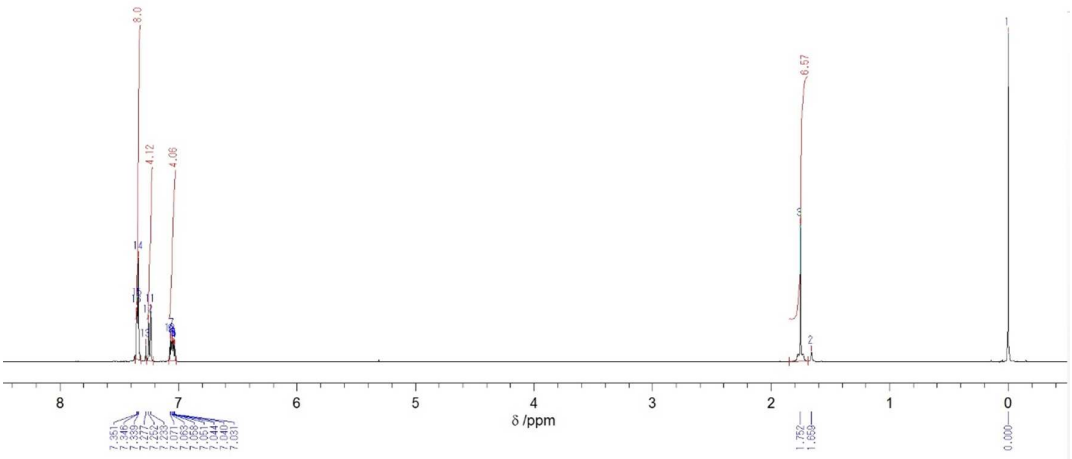

Figure S5. ^{1}H NMR spectrum (400 MHz) of $[PtCl_2(\mathbf{2})_2]$ in $CDCl_3$.

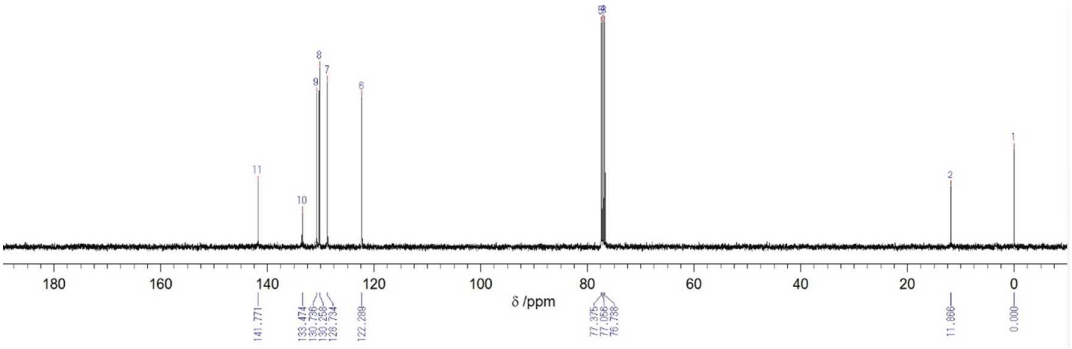

Figure S6. $^{13}C\{^{1}H\}$ NMR spectrum (100 MHz) of $[PtCl_2(\mathbf{2})_2]$ in $CDCl_3$.

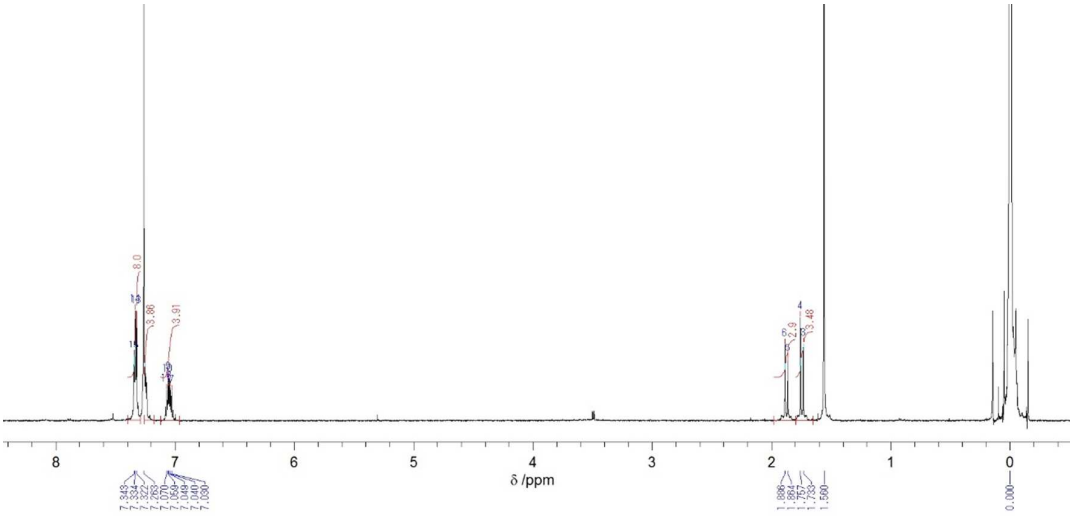

Figure S7. ^{1}H NMR spectrum (400 MHz) of $[PtBr_2(\mathbf{2})_2]$ in $CDCl_3$.

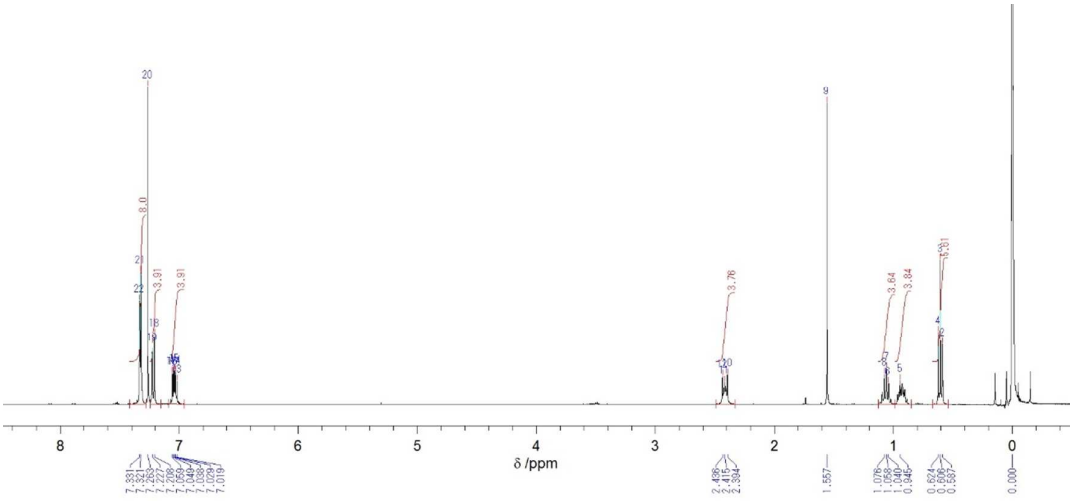

Figure S8. ^{1}H NMR spectrum (400 MHz) of $[PtCl_2(\mathbf{3})_2]$ in $CDCl_3$.

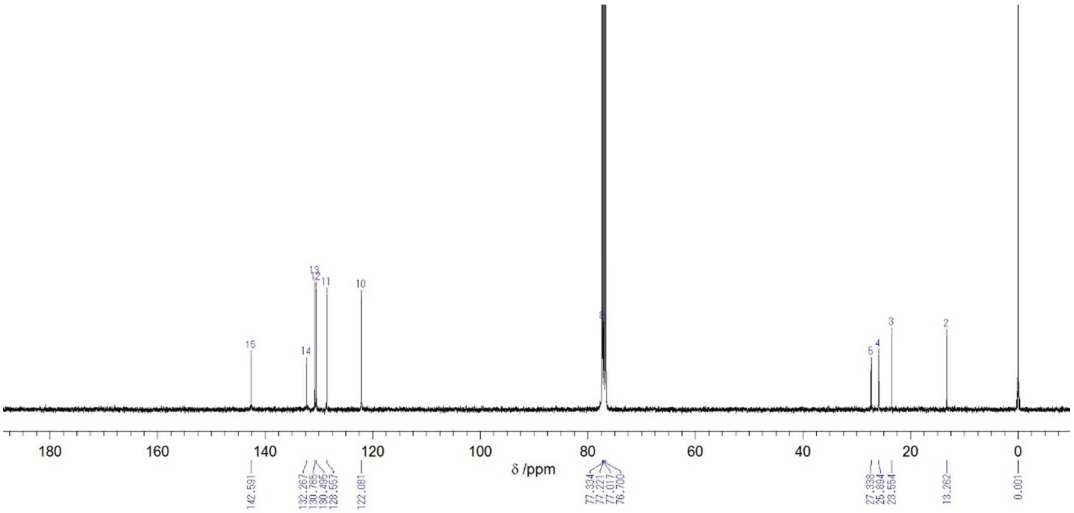

Figure S9. $^{13}C\{^{1}H\}$ NMR spectrum (100 MHz) of $[PtCl_2(\mathbf{3})_2]$ in $CDCl_3$.

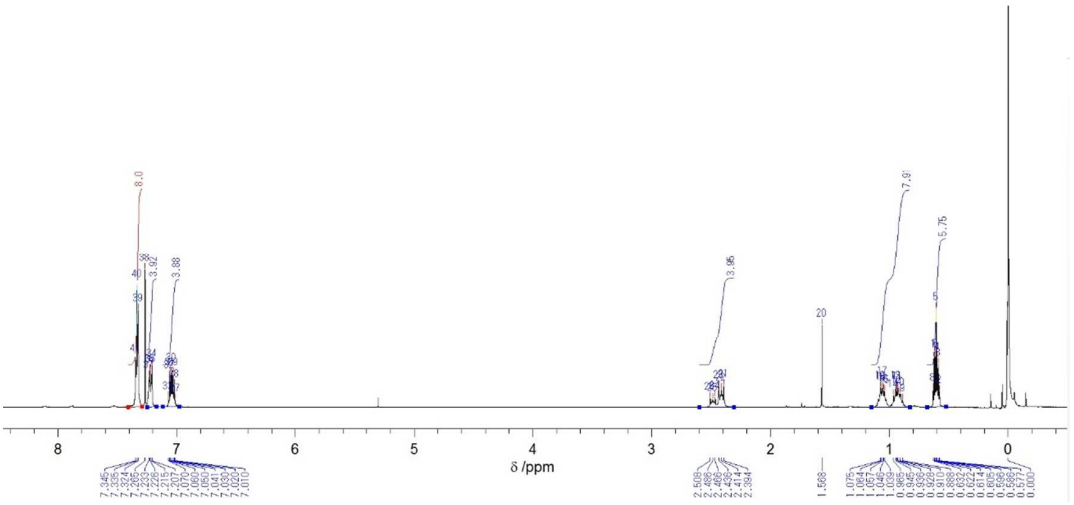

Figure S10. ^{1}H NMR spectrum (400 MHz) of $[PtBr_2(\mathbf{3})_2]$ in $CDCl_3$.

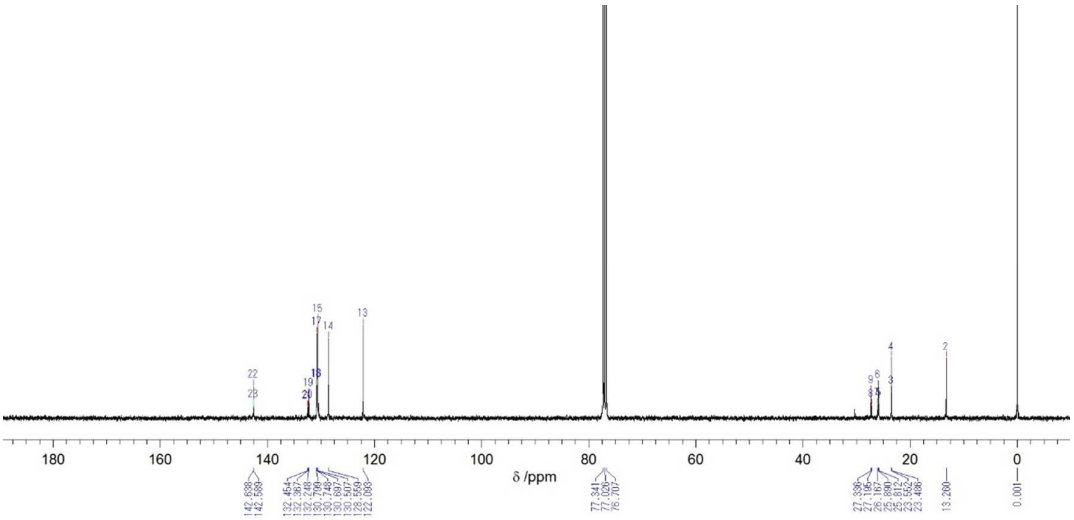

Figure S11. $^{13}C\{^{1}H\}$ NMR spectrum (100 MHz) of $[PtBr_2(\mathbf{3})_2]$ in $CDCl_3$.

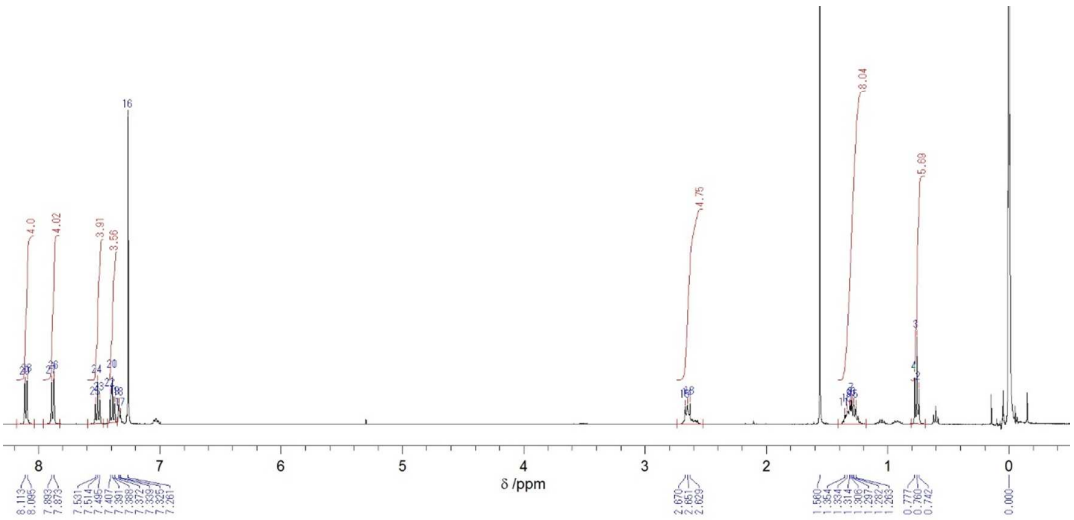

Figure S12. ^{1}H NMR spectrum (400 MHz) of $[PtI_2(\mathbf{3})_2]$ in $CDCl_3$.

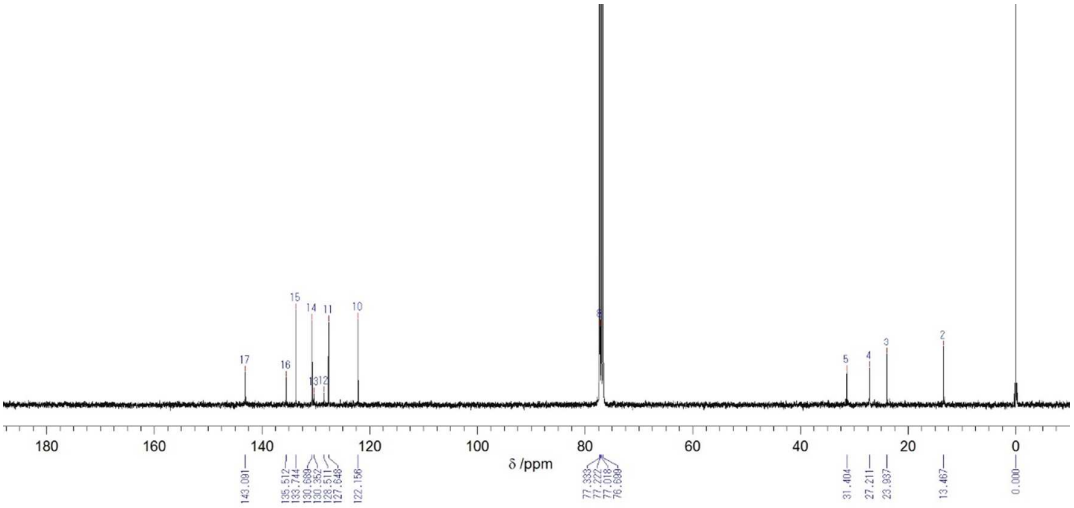

Figure S13. $^{13}C\{^{1}H\}$ NMR spectrum (100 MHz) of $[PtI_2(\mathbf{3})_2]$ in $CDCl_3$.

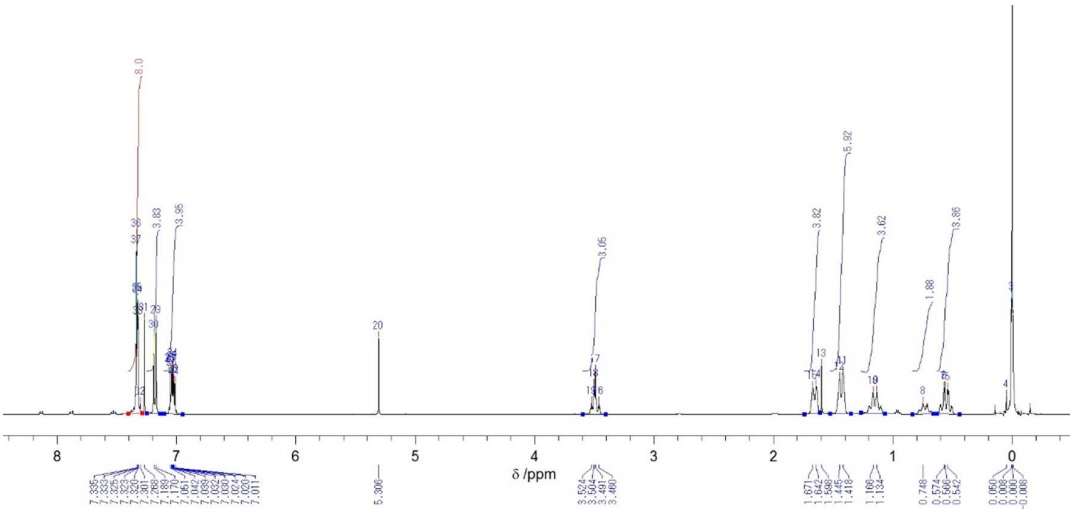

Figure S14. ^{1}H NMR spectrum (400 MHz) of $[PtCl_2(\mathbf{4})_2]$ in $CDCl_3$.

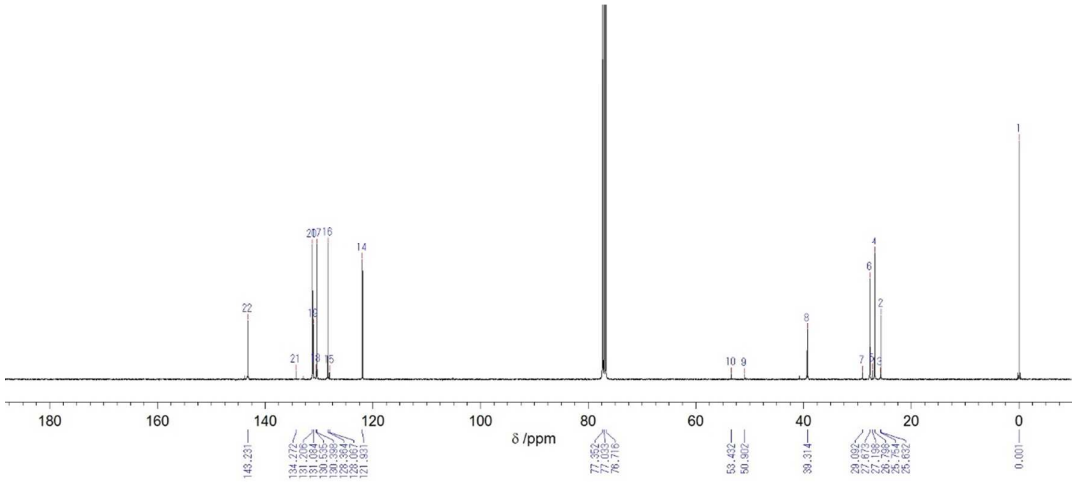

Figure S15. $^{13}C\{^{1}H\}$ NMR spectrum (100 MHz) of $[PtCl_2(\mathbf{4})_2]$ in $CDCl_3$.

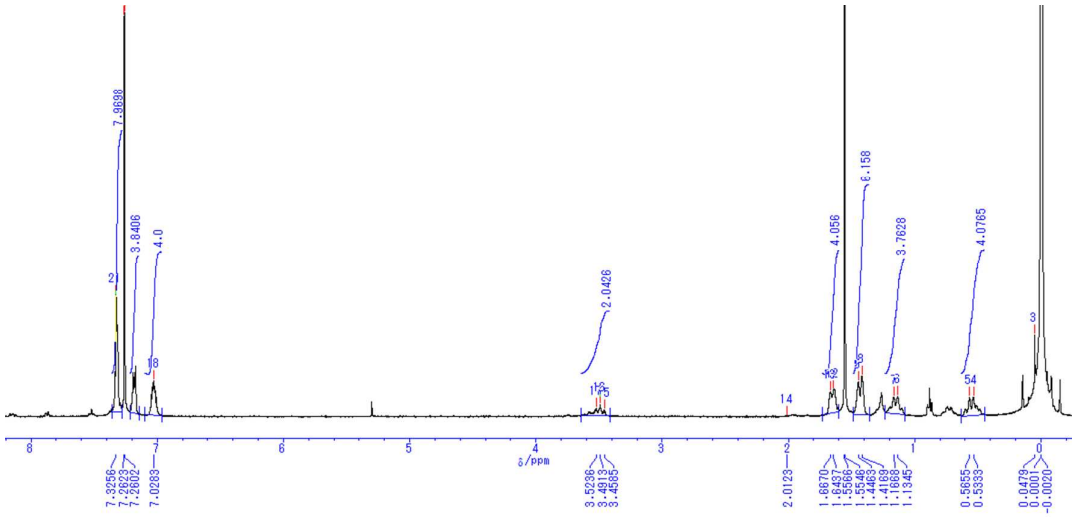

Figure S16. ^{1}H NMR spectrum (400 MHz) of $[PtBr_2(\mathbf{4})_2]$ in $CDCl_3$.

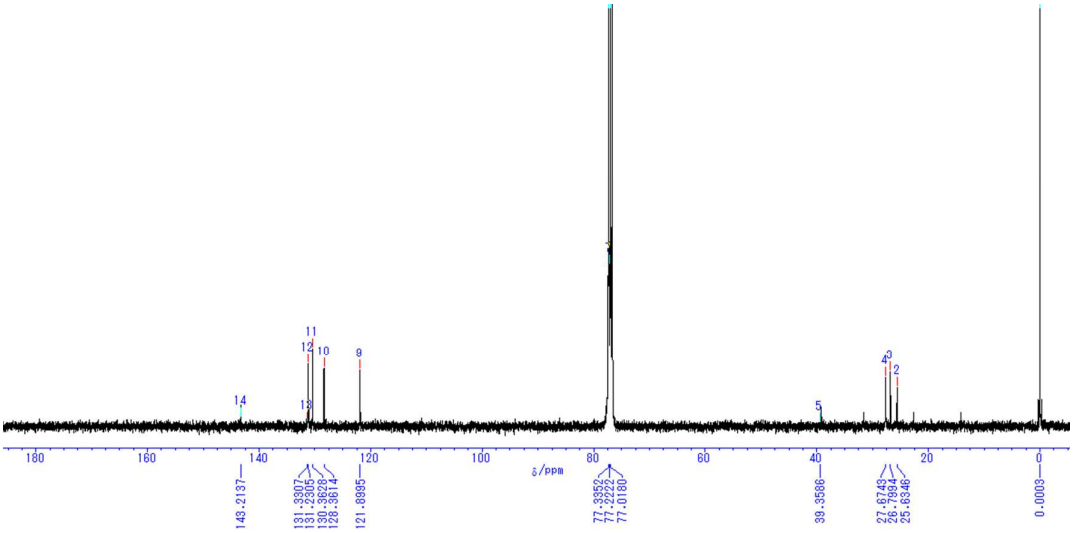

Figure S17. $^{13}C\{^{1}H\}$ NMR spectrum (100 MHz) of $[PtBr_2(\mathbf{4})_2]$ in $CDCl_3$.

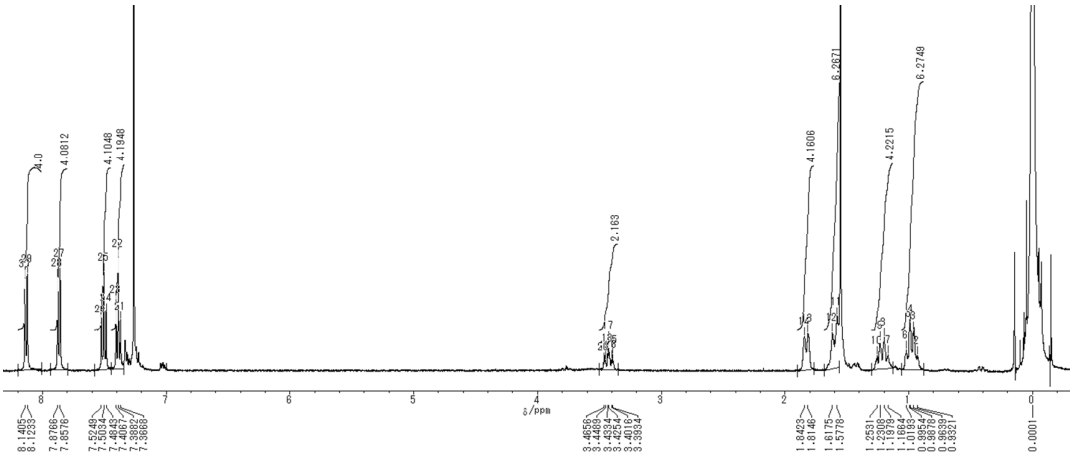

Figure S18. ^{1}H NMR spectrum (400 MHz) of $[PtI_2(\mathbf{4})_2]$ in $CDCl_3$.

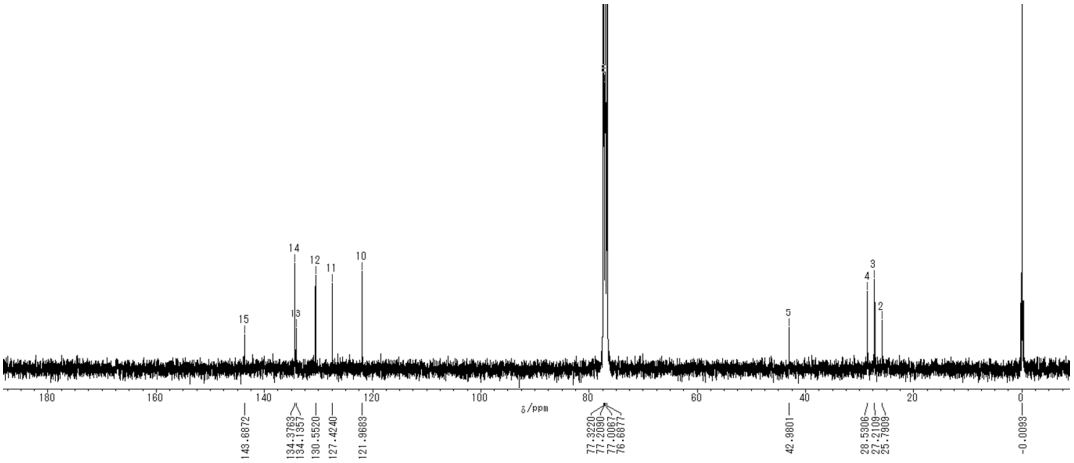

Figure S19. $^{13}C\{^{1}H\}$ NMR spectrum (100 MHz) of $[PtI_2(\mathbf{4})_2]$ in $CDCl_3$.

3. Computational methods

Time-dependent Density functional theory (TD-DFT) calculations with B3LYP functional were employed to investigate the origin of electronic transitions of *cis*- and *trans*-$[PtCl_2(\mathbf{2})_2]$ complexes. For this purpose, single-point energy calculations were performed by using the geometries obtained from the crystallographic studies mentioned above. During the DFT calculations implemented in the Gaussian 09 code[1] we used the CEP-121G basis set for the Pt atoms, and the 6-311G* basis set for the As, C, Cl, and H atoms. Furthermore, ^{1}H NMR shielding tensors of *cis*- and *trans*-$[PtCl_2(\mathbf{2})_2]$ complexes were calculated by gauge-independent atomic orbital (GIAO) B3LYP methods with the same basis sets.

4. Computational data

A. Frontier orbitals of *cis*-[$PtCl_2$(**2**)$_2$] and *trans*-[$PtCl_2$(**2**)$_2$] complexes important for their electronic transition.

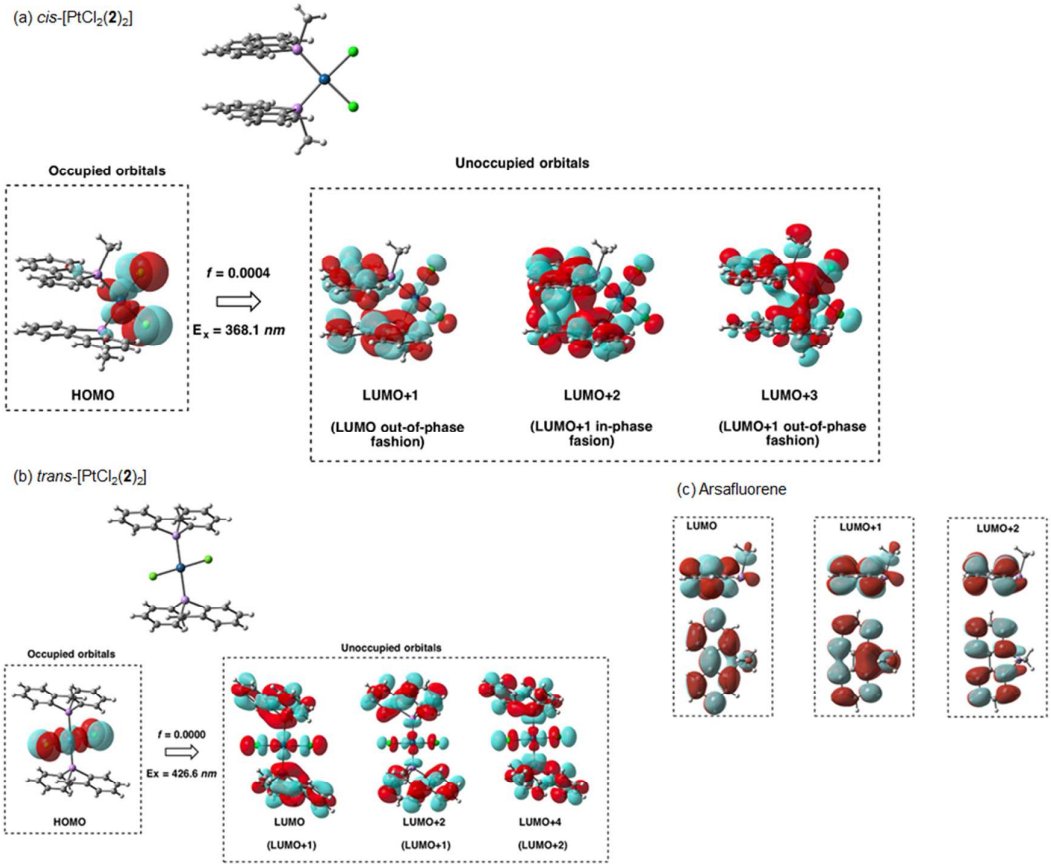

Figure S20. Information of electronic transition in the frontier orbital regions of (a) *cis*- and (b) *trans*-[$PtCl_2$(**2**)$_2$] complexes obtained from TD-DFT calculations, and (c) unoccupied orbitals in frontier orbital regions of arsafluorene. Frontier orbitals in Pt complexes are made up by combinations between two arsafluorene and $PtCl_2$ moieties. The origin of the frontier orbitals in two arsafluorene moieties is given in parentheses. LUMO, LUMO+1, and LUMO+2 described in parentheses means frontier orbitals of arsafluorene.

B. NMR shielding tensor of H atoms of a fluorene moiety of *cis*-[$PtCl_2$(**2**)$_2$] and *trans*-[$PtCl_2$(**2**)$_2$] obtained from GIAO B3LYP methods.

(i) Definition of labels of H atoms of a fluorene moiety

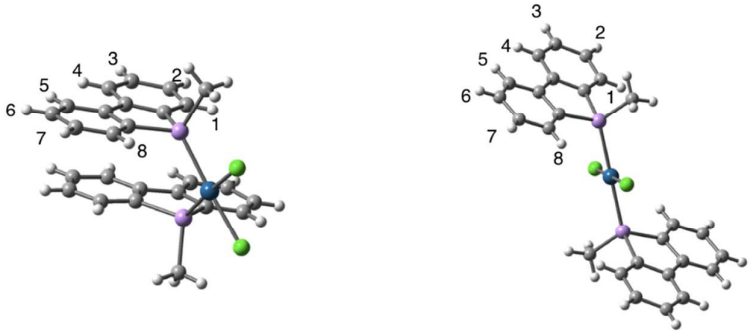

(ii) Calculated NMR shielding tensor of contained H atoms in ppm.

H atom labels	1	2	3	4	5	6	7	8
cis-[$PtCl_2$(**2**)$_2$]	27.8	27.7	27.4	27.3	27.0	26.7	26.7	26.3
trans-[$PtCl_2$(**2**)$_2$]	26.5	27.0	26.7	26.4	26.5	26.7	26.8	26.1

Figure S21. NMR shielding tensor of H atoms of a fluorene moiety of *cis*-[$PtCl_2$(**2**)$_2$] and *trans*-[$PtCl_2$(**2**)$_2$] obtained from GIAO B3LYP methods. (i) Definition of labels of H atoms of a fluorene moiety of the complexes. (ii) Tables listing calculated NMR shielding tensor of contained H atoms. The data indicated that NMR shielding tensors of H atoms contained in the *cis*-[$PtCl_2$(**2**)$_2$] complex can be distinguished from those in the *trans*-[$PtCl_2$(**2**)$_2$] complex.

5. Optical properties

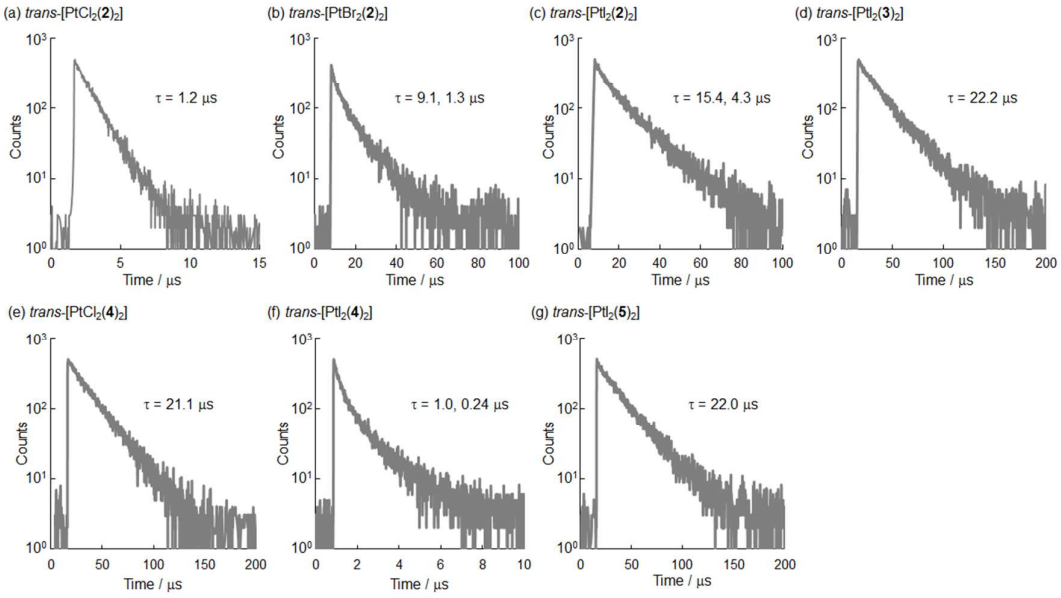

Figure S22. The emission decay kinetics of *trans*-[$PtX_2(L)_2$] (X = Cl, Br, and I, L = **1**-**5**) on excitation at 370 nm (emission wavelength: 640 nm).

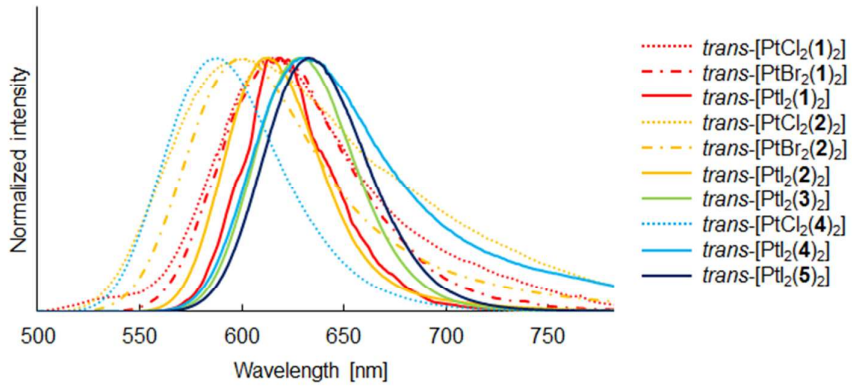

Figure S23. PL spectra (excited at excitation maxima) of *trans*-[$PtX_2(L)_2$].

6. References

[1] Frisch, M. J.; Trucks, G. W.; Schlegel, H. B.; Scuseria, G. E.; Robb, M. A.; Cheeseman, J. R.; Scalmani, G.; Barone, V.; Mennucci, B.; Petersson, G. A.; Nakatsuji, H.; Caricato, M.; Li, X.; Hratchian, H. P.; Izmaylov, A. F.; Bloino, J.; Zheng, G.; Sonnenberg, J. L.; Hada, M.; Ehara, M.; Toyota, K.; Fukuda, R.; Hasegawa, J.; Ishida, M.; Nakajima, T.; Honda, Y.; Kitao, O.; Nakai, H.; Vreven, T.; Montgomery, J. A., Jr.; Peralta, J. E.; Ogliaro, F.; Bearpark, M.; Heyd, J. J.; Brothers, E.; Kudin, K. N.; Staroverov, V. N.; Kobayashi, R.; Normand, J.; Raghavachari, K.; Rendell, A.; Burant, J. C.; Iyengar, S. S.; Tomasi, J.; Cossi, M.; Rega, N.; Millam, J. M.; Klene, M.; Knox, J. E.; Cross, J. B.; Bakken, V.; Adamo, C.; Jaramillo, J.; Gomperts, R.; Stratmann, R. E.; Yazyev, O.; Austin, A. J.; Cammi, R.; Pomelli, C.; Ochterski, J. W.; Martin, R. L.; Morokuma, K.; Zakrzewski, V. G.; Voth, G. A.; Salvador, P.; Dannenberg, J. J.; Dapprich, S.; Daniels, A. D.; Farkas, Ö.; Foresman, J. B.; Ortiz, J. V.; Cioslowski, J.; Fox, D. J. Gaussian 09, Gaussian, Inc.: Wallingford, CT, **2009**.